Topology Optimization Using Basis Functions for Improvement of Rotating Machine Performances

Hidenori Sasaki[1] and Hajime Igarashi[1], *Member, IEEE*

[1]Graduate school of information science and technology, Hokkaido University, Japan

This paper presents a new topology optimization method based on basis functions for design of rotating machines. In this method, the core shape of a given rotating machine is represented by the linear combination of the basis functions. The shape is then freely deformed by changing the weighting coefficients to the basis functions to find the optimal shape. The proposed method is compared with the conventional shape optimization based on polygon morphing. The former is shown to outperform the latter in both IPM and synchronous motor models.

***Index Terms*—Topology Optimization, Basis Function, Polygon Morphing, Finite Element Method**

I. Introduction

In the topology optimization of a rotating machine, the core shape is freely deformed allowing appearance and disappearance of flux barriers and magnets etc. without introducing design parameters unlike the conventional parameter optimizations [1]-[3]. It has been shown that simple optimal shapes which are suitable for manufacturing can be obtained by the topology optimization when the material shape is represented through the liner combination of the basis functions [4]. It has been shown that use of the normalized Gaussians as the basis functions is particularly suitable for the topology optimization of rotating machines [5]-[7].

The topology optimization has been carried out mainly aiming at finding novel shapes in the initial design phase. In the following design phases, on the other hand, it is often required to modify the given core shapes for further improvement of performance such as average torque and efficiency. The topology optimization would also be useful for this purpose because the optimal solution can be explored by flexibly deforming the original core shape.

In this paper, we introduce a new topology optimization method based on the basis functions which modifies the given core shapes of rotating machines. In this method, the material attribute {iron, air} in each finite element in the core is determined from the value of the linear combination of the basis functions. The given motor shape is represented by the basis functions. Then, the weighting coefficients are optimized so that the cost function is minimized under the given constraints. The proposed method is applied to optimization of the rotors of an IPM motor and a synchronous reluctance motor (SynRM). Moreover, the performance of the proposed method is compared with the conventional shape optimization method based on polygon morphing.

Manuscript received June 27, 2017. Corresponding author: H. Sasaki (e-mail: sasaki@em.ist.hokudai.ac.jp).

Digital Object Identifier (inserted by IEEE).

II. Optimization Methods

A. Topology Optimization Using Normalized Gaussians

Although any basis functions can be used in the proposed method, we employ here the normalized Gaussians which are schematically shown in Fig.1. The core of a rotating machine is assumed to be subdivided into finite elements. The material attribute A_e of a finite element in the design region are determined from the value of the shape function defined by

$$\phi(\boldsymbol{x}) = \sum_{i=1}^{N_g} w_i b_i(\boldsymbol{x}) \tag{1}$$

where w_i, $\boldsymbol{x}$ and N_g are the weighting coefficient, gravitation center of the finite element and number of basis functions G_j, respectively, and b_i denotes the normalized Gaussian function given by

$$b_i(\boldsymbol{x}) = G_i(\boldsymbol{x}) \Big/ \sum_{j=1}^{N_g} G_j(\boldsymbol{x}), \tag{2}$$

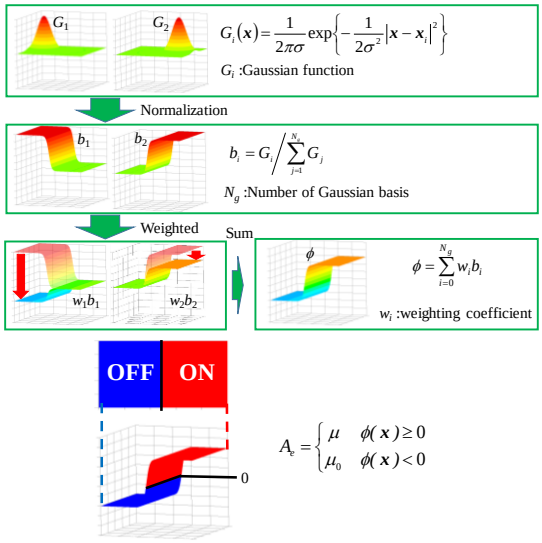

Fig.1 On/off method using normalized Gaussians

$$G_i(\boldsymbol{x}) = \frac{1}{2\pi\sigma}\exp\left\{-\frac{1}{2\sigma^2}|\boldsymbol{x}-\boldsymbol{x}_i|^2\right\}, \quad (3)$$

where σ^2 denotes the variance whose value is set to $\sigma^2=10^{-6}$ mm^2 in the following examples and x_i is the center of Gaussian basis G_i. The material attribute A_e of finite element e in the design region is determined from the shape function ϕ as follows:

$$A_e \leftarrow \begin{cases} \text{iron} & \phi(\boldsymbol{x}) \geq 0, \\ \text{air} & \phi(\boldsymbol{x}) < 0. \end{cases} \quad (4)$$

We determine N_g, σ so that the result has smooth boundaries and also satisfactory performance. The influence of these parameters on the optimal solution has been discussed in [6]. We use Real-coded Genetic Algorithm (RGA) for optimization of w_i.

B. Shape Fitting to Given Model

Fig.2 shows the flow diagram of the proposed method. In the first phase, we determine w_i by RGA so that the model shape represented by ϕ is as near to the base model as possible. For this purpose, we solve the optimization problem defined by

$$N \rightarrow min. \quad (5)$$

where N is the number of finite elements which are inconsistent with the base model.

In the second phase, we add random noises to the gene, $\boldsymbol{w}^t = [w_1, w_2, \ldots, w_{Ng}]$, of the individuals in the initial population for free deformation. Then we start the RGA process for topology optimization [6, 7] as described in *D*.

C. Shape Optimization Based on Polygon Morphing

In order to verify the merit of the proposed method, we compare it with a conventional shape optimization method applied to the base model. This method is schematically shown in Fig.3. We assign vertices on the material boundary of the base model. The coordinates of these vertices are chosen as the genes in RGA. Then, we add random noises to the gene of the individual in common with the proposed method. In the process of RGA, we reject the individuals which have either edge crossing or vertex outside the design region. The material attribute in each finite element in the core is determined from the vertex placement; if the gravitation center of a finite element is inside the polygon defined by the vertices, its material attribute is set to air. Note that this method cannot perform the *topology* optimization because flux barriers do not newly appear or disappear.

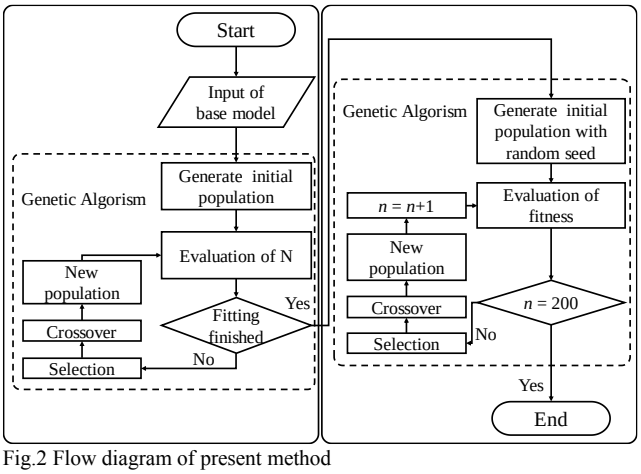

Fig.2 Flow diagram of present method

D. Optimization Setting

Fig. 4(a) shows an IPM motor [8], on the basis of which we construct the base models of IPM and SynRM for optimization. By solving (5), the base models are represented by ϕ in (1) as shown in Fig.4 (b) and (c). These base models of IPM and SynRM have average torques 2.08Nm, 1.28Nm, respectively. For SynRM, the rotor shape shown in Fig.4 (c) has been widely used as can be seen, e.g., in [9]. Fig.5 shows the polygons with 14 and 36 vertices arranged to represent the IPM and SynRM

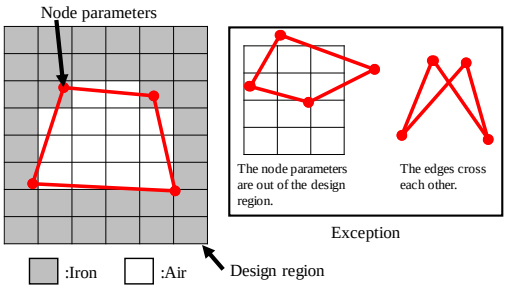

Fig.3 Polygon morphing on/off method

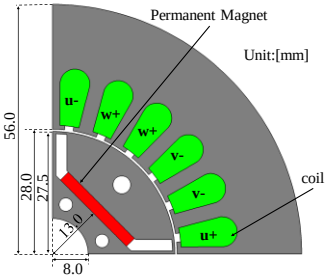

T^0_{ave} = 2.08Nm, T^0_{rip}= 0.57

(a) Base model of IPM motor

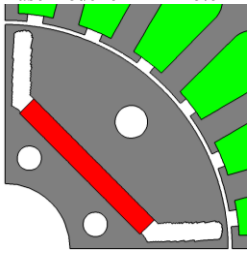
T_{ave} = 1.94Nm, T_{rip}= 0.32

(b) Base model of IPM represented by ϕ.

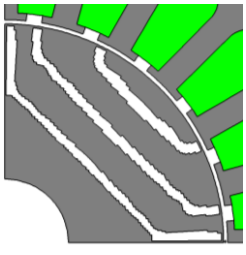
T_{ave} = 1.28Nm, T_{rip}= 0.45

(c) Base model of SynRM represented by ϕ.

Fig.4 IPM motor and base models represented by Gaussian bases

TABLE I.
ROTATING MACHINE PARAMETERS

	IPM	SynRM
Current phase angle [degree]	30	45
Current effective value [A]	4.2425	8.4850
Number of turns [turn]	35	35
Residual flux density [T]	1.25	-

models. The rotating machine parameters and optimization setting are summarized in TABLEs. I and II.

The optimization problem is defined by

$$F = \frac{T_{ave}}{T^0_{ave}} \rightarrow \max.\ \text{sub. to}\ , T_{rip} < T^0_{rip}, N_{\text{area}} < 2, \quad (6)$$

where, T_{ave}, T_{rip}, T^0_{ave} and T^0_{rip} are the average torque, torque ripple and the corresponding values of the IPM motor shown in Fig.4 (a), respectively. The torque ripple is defined by

$$T_{rip} = \frac{T_{max} - T_{min}}{T_{ave}} \quad (7)$$

where $T_{\max}$ and $T_{\min}$ are the maximal and minimal average torque, respectively. Moreover, N_{area} is the number of separated rotor cores. The FE analysis of magnetic fields by fine mechanical angular interval $\Delta\theta$ gives rise to long computational time. For this reason, we set $\Delta\theta = 5$ degrees for the optimization. Because the algorithm almost converges at 200 generations, we stop the RGA process at this point in all the cases.

III. Optimization Results

A. Optimization of IPM motor

Fig. 6 shows the resultant rotor shapes of the IPM motor obtained by the topology optimization with Gaussian basis functions and shape optimization based on polygon morphing, which will be referred to as topology and shape optimizations, respectively. The new flux barriers appear near the rotor surface only in (a), while the flux barriers beside the magnet expand by the optimization in a similar way in both (a) and (b). The average torque is improved from 2.08Nm to 2.37Nm and 2.27Nm by the topology and shape optimizations, respectively, from which it is concluded that the former result is about 5% better.

TABLE II.
PARAMETERS IN OPTIMIZATION.

	Gaussian bases		Polygon Morphing	
	IPM	SynRM	IPM	SynRM
Number of genes	73	87	28	72
Number of individuals	810	1800	600	810
Number of children	270	360	120	270
Number of generations	200	200	200	200
Maximum of noises	1.0×10^{-2} / 5.0×10^{-2}		1.0×10^{-4} / 5.0×10^{-2}	

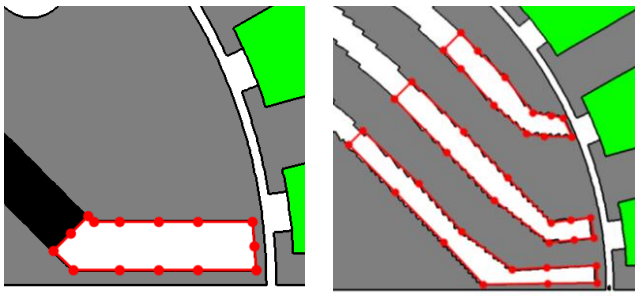

(a) Base model of IPM motor represented by a polygon (b) Base model of SynRM represented by polygons

Fig.5 Shape optimization based on polygon morphing

Fig. 7 shows the magnitude of magnetic induction and lines of magnetic flux. There are magnetic saturations between the rotor surface and the small flux barrier in (a). This magnetic satuartion would relux the variation of the magnetic induction in the azimuthal direction and supress the torque ripple. Fig. 8 shows the torque waveforms. The computing time for the fitting is about 7 hours and 2 days for topology and polygon morphing optimizations, respectively, when using Intel Xeon CPU E5-2650 v2 at 2.6GHz (2×8 cores in total).

To consider dependence of the convergent solution on the random seed, we perform the topology optimization for different five seeds. The resultant average torque is 2.43Nm and the standard deviation is 1.19×10^{-1} Nm. For this results, we conclude that the optimal solutions do not have significant impacts in their performance for different random seeds when starting from the base model.

B. Optimization of SynRM

Fig. 9 shows the resultant rotor shapes of SynRM obtained by the topology and shape optimizations. The width of the flux

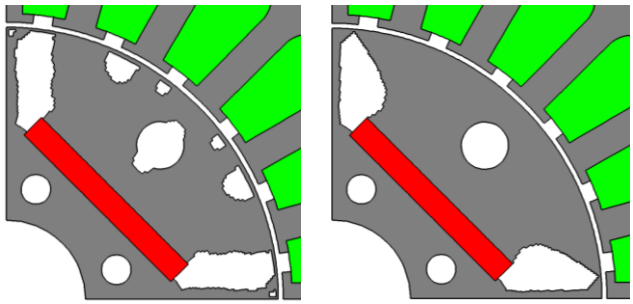

T_{ave} = 2.37Nm, T_{rip}= 0.28 T_{ave} = 2.27Nm, T_{rip}= 0.21

(a) Gaussian basis function (b) Polygon morphing

Fig.6 Optimized shapes of IPM motor

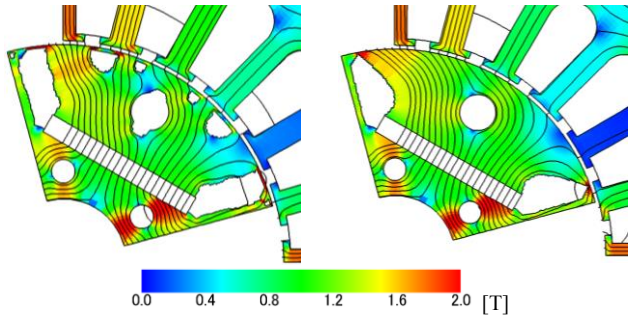

(a) Gaussian basis function (b) Polygon morphing

Fig.7 Magntic induction and flux lines in optimized IPM motors

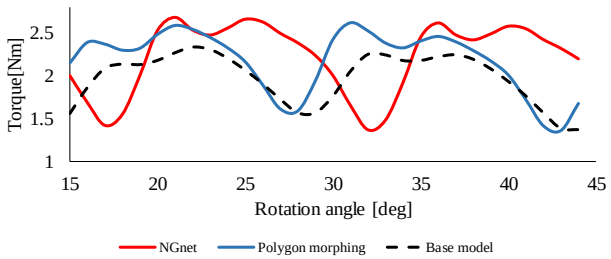

Fig.8 Torque waveforms of IPM motor

barriers increases by the optimization in both (a) and (b). The average torque is improved from 1.28Nm to 2.04Nm and 1.79Nm by the topology and shape optimizations, respectively, from which it is concluded that the former result is about 14% better. Fig. 10 shows the magnitude of magnetic induction and lines of magnetic flux. The magnetic fluxes pass through the U-shaped bridges in both resultant rotors. Fig. 11 shows the torque waveforms. The torque of SynRM optimized by the toplogy optimization is found to be clearly stronger than other two torques.

C. *Smoothing of material boundaries*

Although smooth material boundaries are preferable for the manufacturing, the topology optimization often gives rise to complicated material boundaries. For this reason, the resultant material boundaries would be made smooth after the optimization process. To investigate the effect of the material smoothing on the torque characteristic, the rotor resulted from the topology optimization is made smooth as shown in Fig.12. The core shape is represented now by polygons with vertices, marked by red points. The torque waveforms before and after smoothing are comparatively plotted in Fig.13. It can be seen that there are little differences between the two curves.

IV. Conclusion

In this paper, we have proposed a topology optimization method starting from a given core shape. This method can be used for improvement of existing machine models. The topology optimization in which the rotor shape is represented by the Gaussian basis functions outperforms the conventional shape optimization based on polygon morphing for IPM motor and SynRM models. Smoothing of the material boundary in the rotor optimized by the topology optimization gives little changes in the torque characteristics.

References

[1] Y. Okamoto et al., "Topology optimization of rotor core combined with identification of current phase angle in IPM motor using multistep genetic algorithm," IEEE Trans. Magnetics, vol. 50, no. 2, 2014.

[2] N. Takahashi et al, "Optimization of rotor of actual IPM motor using ON/OFF method," IEEE Trans. Magnetics, vol. 47, no. 5, pp. 1262-1265, 2011.

[3] Y. Hidaka, T. Sato, H. Igarashi, "Topology Optimization Method Based on On-Off Method and Level Set Approach," IEEE Trans. Magnetics, vol. 50, no. 2, pp. 617-620, 2014.

[4] Y. Tsuji and K. Hirayama, "Design of optical circuit devices using topology optimization method with function-expansion-based refractive index distribution," IEEE Photon. Technol. Lett., vol. 20, no. 12, pp. 982-984, Jun. 2008.

[5] T. Sato et al., "A modified immune algorithm with spatial filtering for multiobjective topology optimization of electromagnetic devices," COMPEL, vol. 33, no.3, pp. 821-833, 2014.

[6] T. Sato, K. Watanabe, and H. Igarashi, "Multimaterial Topology Optimization of Electric Machines Based on Normalized Gaussian Network," IEEE Trans. Magnetics, vol. 51, no. 3, pp. 1-4, 2015.

[7] S. Sato, T. Sato, and H. Igarashi, "Topology optimization of synchronous reluctance motor using normalized Gaussian network," *IEEE Trans*. Magnetics, vol.51, no.3, 2015.

[8] Technical report of the institute of electrical engineering of Japan, industry application society, No. 776, 2000.

[9] H. Murakami et al., "The performance comparison of SPMSM, IPMSM and SynRM in use as air-conditioning compressor," in Proc. Conf. Rec. IEEE 34th IAS Annu. Meeting Ind. Appl. Conf., Oct. 1999, pp. 840–845.

[10] T. Kobayashi, Y. Takeda, M. Sanada, S. Morimoto, "Vibration Reduction of IPMSM with Concentrated Winding by Making Holes," *IEEJ Trans. on Industry Applications*, vol. 124, no.2, 2004(in Japanese).

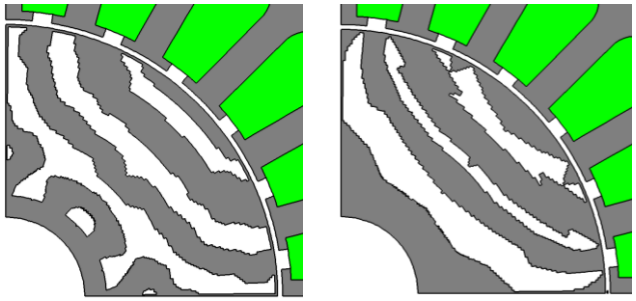

T_{ave} = 2.04Nm, T_{rip}= 0.27 T_{ave} = 1.79Nm, T_{rip}= 0.21

(a) Gaussian basis function (b) Polygon morphing

Fig.9 Optimized shapes of SynRM

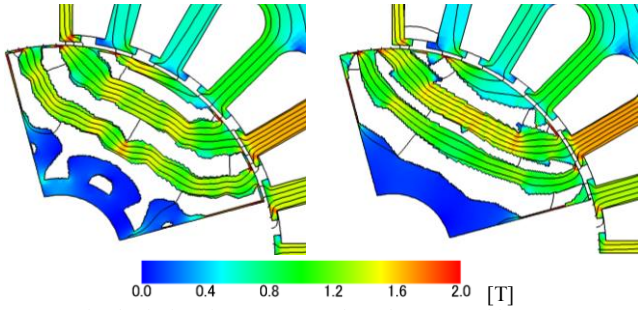

(a) Gaussian basis function (b) Polygon morphing

Fig.10 Magntic induction and flux lines in optimized SynRM

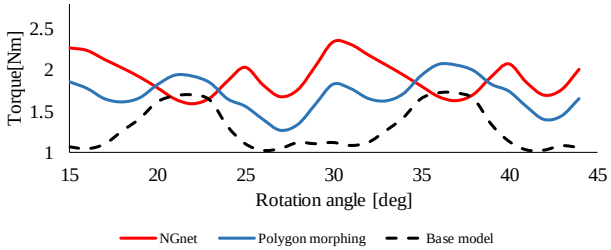

Fig.11 Torque waveforms of synchronous reluctance motor

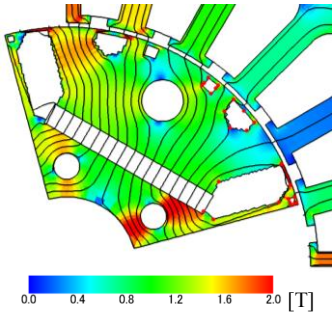

Fig.12 Smooting of material bounraies

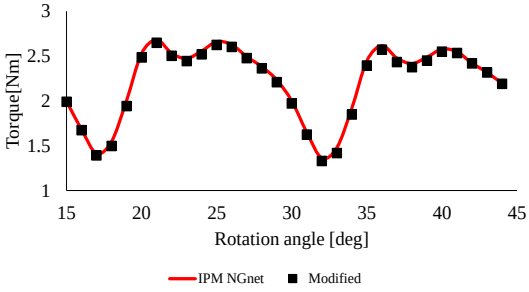

Fig.13 Effect of smooting